Chemical Engineering Journal 450 (2022) 138037

Contents lists available at ScienceDirect

Chemical Engineering Journal

journal homepage: www.elsevier.com/locate/cej

How can a hydrophobic polymer PTAA serve as a hole- transport layer for an inverted tin perovskite solar cell?

Chun-Hsiao Kuan [a], Guo-Shao Luo [a], Sudhakar Narra [a,b], Surajit Maity [a], Hirotsugu Hiramatsu [a,b], Yi-Wei Tsai [c], Jhih-Min Lin [c], Cheng-Hung Hou [d], Jing-Jong Shyue [d,e], Eric Wei-Guang Diau [a,b,*]

[a] Department of Applied Chemistry and Institute of Molecular Science, National Yang Ming Chiao Tung University, 1001 Ta-Hsueh Rd., Hsinchu 30010, Taiwan
[b] Center for Emergent Functional Matter Science, National Yang Ming Chiao Tung University, 1001 Ta-Hsueh Rd., Hsinchu 30010, Taiwan
[c] National Synchrotron Radiation Research Center, 101 Hsin-Ann Road, Hsinchu Science Park, Hsinchu 30076, Taiwan
[d] Research Center for Applied Sciences, Academia Sinica, Taipei 11529, Taiwan
[e] Department of Materials Science and Engineering, National Taiwan University, Taipei 10617, Taiwan

A B S T R A C T

We deposited a smooth and uniform tin-perovskite layer on a hydrophobic conducting polymer, (bis (4-phenyl) (2,4,6-trimethylphenylamine) (PTAA), on modification of the PTAA surface with an organic ammonium salt, phenylethylammonium iodide (PEAI), according to a two-step approach. We found that π-π interaction between the phenyl rings of PTAA and PEAI plays an important role to modify the hydrophobicity of the PTAA surface and to passivate the crystal surface so as to form a tin-perovskite film of high quality. The $FASnI_3$ device with PTAA serving as a hole-transport layer (HTL) attained PCE 8.3 % with great stability, becoming the first example reported for a PTAA-based tin-perovskite solar cell. Our approach is applicable to other prospective HTL materials to match the energy levels between perovskite and HTL so as to enhance further the performance of the device.

1. Introduction

Perovskite solar cells (PSC) attract much attention due to the rapid progress of their device performance toward the level of silicon-based solar cells [1,2], but traditional perovskites contain toxic lead element that must be removed for their environmentally benign development. A tin-perovskite solar cell (TPSC) has thus emerged as a prospective candidate to serve lead-free photovoltaic applications [3]. Recent progress in the performance of a TPSC has been remarkable; the efficiency of power conversion (PCE) increased from 6.22 % in 2016 up to 14.8 % in 2021 based on an inverted device architecture [4]. Furthermore, almost all high-performance TPSC were fabricated using poly(3,4-ethylenedioxythiophene):poly(styrene sulfonate) (PEDOT:PSS) as a hole- transport layer (HTL) according to a one-step deposition method [3,4,5,6,7,8]. Because the reaction between the precursors (SnI_2 and FAI; FA represents formamidinium) is rapid, polar solvent dimethyl sulfoxide (DMSO) was used in the precursor solution to form intermediate adducts with SnI_2 so that crystallization became effectively retarded [5,9]. The hydrophilic HTL-like PEDOT:PSS in a p-i-n device structure [10], enhanced the interaction with the perovskite precursor solution so as to increase the rate of nucleation and to decrease the rate of crystallization [3]. PEDOT:PSS is, however, hygroscopic and readily adsorbs water from the environment to degrade the stability of a device. To solve this problem, in addition to the modification of PEDOT:PSS [11,12], one might consider a hydrophobic conducting polymer such as poly(bis(4-phenyl) (2,4,6- trimethylphenylamine) (PTAA) to replace PEDOT:PSS in serving as a HTL to improve the stability of the TPSC. PTAA has been widely applied to serve as a HTL for an inverted lead PSC [13,14]. The best performance of a lead-based PSC attained PCE 22.3 % [15]. In contrast, to our best knowledge, there has been no report of using PTAA as a HTL for TPSC due to the hydrophobic nature of PTAA and rapid crystallization rate of the tin perovskite, which makes it difficult for tin perovskite to form a uniform layer on PTAA according to a traditional one-step deposition approach.

We recently developed a two-step deposition method to fabricate a smooth and uniform tin-perovskite layer on the surface of PEDOT:PSS [16], or on a hole-selective self-assembled monolayer (SAM) [17]. In the two-step approach [9,16,17], precursor SnI_2 was deposited first; then another precursor FAI followed. In this way, the nucleation became controlled by the interaction between SnI_2 and HTL in the first step; the crystal growth became controlled via delayed addition of FAI in the second step. The two-step method has hence the potential to grow a

* Corresponding author at: Department of Applied Chemistry and Institute of Molecular Science, National Yang Ming Chiao Tung University, 1001 Ta-Hsueh Rd., Hsinchu 30010, Taiwan.
E-mail address: diau@nycu.edu.tw (E. Wei-Guang Diau).

https://doi.org/10.1016/j.cej.2022.138037
Received 10 May 2022; Received in revised form 27 June 2022; Accepted 8 July 2022
Available online 11 July 2022

uniform tin-perovskite layer on a hydrophobic HTL surface if the first deposition step can be well managed. In the present work, we demonstrate for the first time the fabrication of a PTAA-based TPSC using a two-step method. The key factor is the modification of the hydrophobic surface of PTAA with a suitable organic ammonium cation, phenylethylammonium iodide (PEAI), so that the modified PTAA surface becomes hydrophilic for feasible deposition of the SnI_2 precursor in the first step. As shown in Fig. 1, because the phenyl group is lipophilic, the phenyl ring of PEAI likely interacts with PTAA through a π-π stacking effect to adjust the hydrophobicity of the surface. As a result, a uniform tin-perovskite layer $FASnI_3$ can be produced with no pinhole; the device performance in an inverted structure attained PCE 8.3 %.

We first demonstrate the effect of PEAI applied for fabrication of tin-perovskite films using either a traditional one-step [18], or our newly developed two-step method [16,17]. As the photographic images of the films show in Figure S1a, the one-step process of tin perovskite on PTAA cannot form a perovskite layer because the non-polar anti-solvent would easily wash away the spin-coated precursor. The two-step process improved the film formation but many pinholes were also produced (Figure S1b). When the PTAA surface was modified with PEAI, the one-step process produced a black tin-perovskite phase but also pinholes (Figure S1c). When the two-step process was applied on the PEAI-modified PTAA surface, a smooth and pinhole-free tin perovskite film was produced (Figure S1d). Figures S2a and b show side-view SEM images of the tin- perovskite films produced via the two-step deposition method without and with a PEAI modification, respectively. The film generated without PEAI pretreatment shows great roughness with film thickness ~ 100 nm (Figure S2a). In contrast, with PEAI pretreatment, the film thickness was significantly enhanced to ~ 250 nm (Figure S2b) with a film quality much improved relative to that without a PEAI pretreatment.

PTAA has a symmetrical polymer structure with one N atom connected with three phenyl rings. As shown in Fig. 1, the phenyl rings of PTAA interact with that of PEAI through a π-π interaction, which modifies the hydrophobic surface of PTAA and helps to regulate the large surface tension of PTAA. Fig. 2a and b show atomic-force microscope (AFM) images of PTAA and PEAI-modified PTAA films, respectively. These results show that the PTAA film was evenly distributed on the ITO substrate (Fig. 2a). After spin-coating of a thin layer of PEAI on PTAA, the PTAA surface was, however, only partially covered with PEAI as some smooth areas of PEAI are clearly visible in the AFM image in Fig. 2b. For the PEAI to cover the entire PTAA surface is unnecessary because the purpose of functionalization of the PTAA surface with PEAI is to make a hydrophilic surface with diminished surface tension for feasible deposition of a tin perovskite layer. When the PTAA surface becomes hydrophilic, the SnI_2/DMSO solution can spread smoothly on the PTAA surface ready for rapid nucleation of perovskite nanocrystals to proceed. This effect is visible in the plots of contact angles [19]; the contact angle of the SnI_2/DMSO droplet on pristine PTAA is 42.42° (Fig. 2c) whereas it decreased significantly to 5.97° when the SnI_2/DMSO precursor solution was dropped onto the PTAA-PEAI surface (Fig. 2d). In addition, the ammonium cationic terminal of PEAI interacted with the SnI_2 and FAI precursors to grow the perovskite crystals smoothly and to stabilize the perovskite phase when the FAI/co-solvent precursor was spin-coated in the second step [10]. As a result, the two-step method without PEAI pretreatment produced a blurred tin-perovskite film containing some pinholes on the pristine PTAA layer (Fig. 2e), whereas uniform and close-packed tin perovskite crystals were unambiguously produced on the PEAI-modified PTAA surface (Fig. 2f). Film roughness is also an important issue to be considered. Figures S3a and b show AFM images for tin-perovskite films produced without and with PEAI pretreatment, respectively. It can be seen that the perovskite film grown on the pristine PTAA surface without PEAI modification displays great roughness (~45 nm), whereas the roughness of the PEAI-modified perovskite film became significantly decreased (~33 nm). The results from analysis of the AFM data of the two samples are summarized in Table S1. We noticed also that the size of the crystal grains of the PEAI-treated tin-perovskite film became significantly enhanced to an average value 570 nm, which is much greater than that (240 nm) fabricated without PEAI pretreatment; plots of their corresponding size distributions appear in Figure S4.

The crystal structure of tin perovskite fabricated with the two-step method without and with PEAI pretreatment was investigated using X-ray diffraction (XRD) and grazing-incidence wide-angle X-ray scattering (GIWAXS) techniques. Figure S5 shows XRD patterns for films made of $FASnI_3$ on PTAA and $FASnI_3$ on PTAA-PEAI. PEAI is typically added to the tin-perovskite precursor solution to form a 3D/2D hybrid structure [20], but in our case the characteristic XRD signals for both tin-perovskite films are similar and no 2D phase in the region of small diffraction angles was found for the PTAA-PEAI film. The GIWAXS images which was taken at the beamline TLS 23A1 in National Synchrotron Radiation Research Center (NSRRC), Taiwan, for films made of PTAA only, PTAA-PEAI, $FASnI_3$ on PTAA and $FASnI_3$ on PTAA-PEAI are shown in Figures S6a-d, respectively. The incident angle is 0.2°and the excitation energy is 10.0 keV. We found that there were apparent 2D patterns corresponding to facets (0 0 1) and (0 0 2) for the PTAA-PEAI film

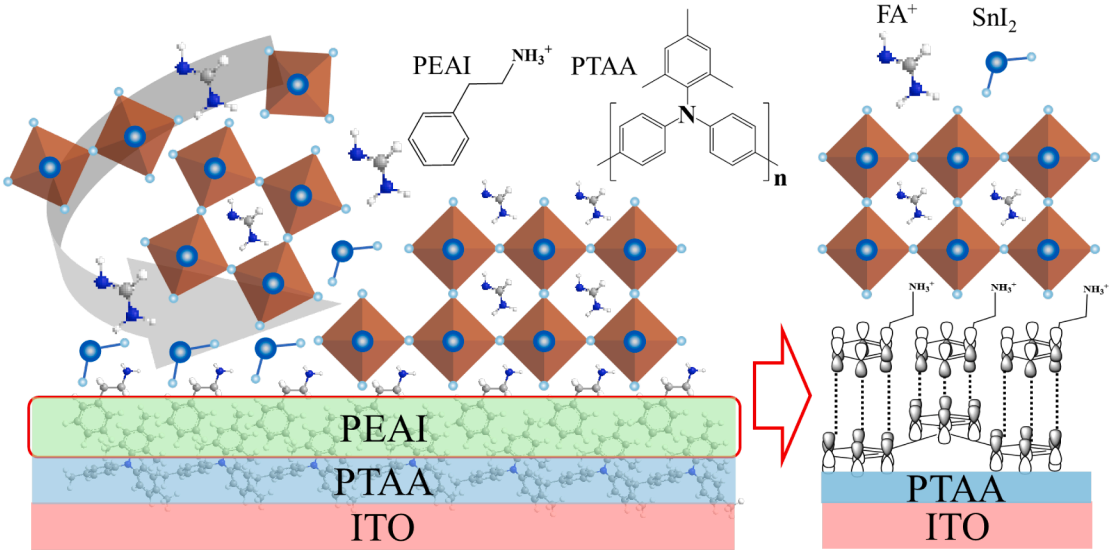

Fig. 1. Schematic demonstration of π-π stacking effect in the interface between PTAA and PEAI.

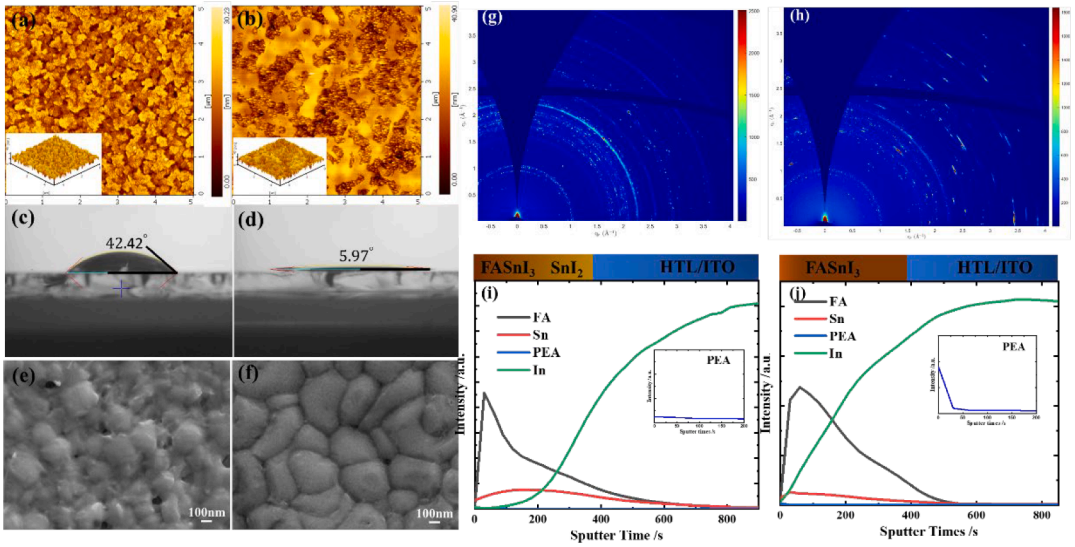

Fig. 2. AFM images of (a) PTAA and (b) PTAA-PEAI films; plots of contact angle of SnI_2/DMSO solution dropped onto (c) PTAA and (d) PTAA-PEAI surfaces; SEM images of $FASnI_3$ fabricated with a two-step method on (e) PTAA and (f) PTAA-PEAI surfaces; GIWAXS of $FASnI_3$ fabricated on (g) PTAA and (h) PTAA-PEAI surfaces; TOF-SIMS of $FASnI_3$ fabricated on (i) PTAA and (j) PTAA-PEAI surfaces.

(Figure S6b). When we grew tin perovskite on the pristine PTAA surface, there appeared some random signals corresponding to both α-phase and δ-phase (Figure S6c). In contrast, when perovskite was grown on the PTAA-PEAI film, only stable α-phase (1 0 0) was observed (Figure S6d).

Furthermore, the GIWAXS images were obtained at a higher energy (12.37 keV) and a lower incident angle (0.01°) at the beamline TPS 25A1 in NSRRC. The footprint of the X-ray beam on the samples was only a few mm in TPS 25A1. Due to the low incident angle and the small footprint, the diffraction from the sample was significantly enhanced. By measuring at incident angle 0.01°, we were able to observe the structural feature exclusively on the top surface of the crystal. As the dotted patterns shown in Fig. 2g, the orientation of perovskite surface on PTAA is random and disperse [21,22]. In contrast, as dashed patterns shown in Fig. 2h, the perovskite produced on the PTAA-PEAI surface shows well-organized crystal feature with large grain size and high crystallinity. This is consistent with the SEM image showing larger and well packed crystals for the latter than for the former. Both XRD and GIWAXS results confirmed that there was no 2D perovskite crystal structure produced on the 3D perovskite surface.

In order to further find out the role of PEAI and validate the completeness of the SnI_2 and FAI reaction after the PEAI pretreatment, we carried out time-of-flight secondary-ion mass spectroscopy (TOF-SIMS) analysis to reveal the spatial distribution of each component. The distributions of each cation species for the tin perovskite made on PTAA only and PEAI treated PTAA films are shown in Fig. 2i and j, respectively. PEA^+ was found on the top surface of perovskite of the PTAA-PEAI film as shown in the TOF-SIMS depth profile (inset of Fig. 2j). It suggests that PEAI provided π-π interaction with PTAA and then dispersed to the bulk region and finally moved to the top surface of perovskite through diffusion, consistent with the small-angle GIWAXS results showing the effect of PEAI passivation to form larger crystals. Judging from the TOF-SIMS results, when making perovskite on the PTAA surface in two steps, excessive SnI_2 could remain in the bottom due to incomplete reaction between SnI_2 and FAI. As shown in Fig. 2i, the signal of FA^+ of perovskite film without PEAI was sharp and cumulated on the top surface of perovskite while the signal of Sn^{2+} increased as the signal of FA^+ decreased, an indication of incomplete reaction. After treating with PEAI (Fig. 4j), both signals of FA^+ and Sn^{2+} become smooth and broad to confirm the complete reaction between FAI and SnI_2.

To confirm the π-π stacking effect between PTAA and PEAI, we recorded Raman spectra of films made of (i) pure PTAA, (ii) pure PEAI and (iii) PTAA + PEAI; the results appear in Fig. 3a. The grey Raman spectrum of (iv) was obtained on subtracting curves of (i) PTAA and (ii) PEAI from (iii) PTAA + PEAI; the black solid trace in (iv) is the result of curve smoothing. The Raman line of PTAA at 1609 cm^{-1} is assignable to the stretching mode of the phenyl rings and the C–N bonds, the line at 1321 cm^{-1} to the C–N and C–C stretching modes [23,24]. In subtracted trace (iv), reversed first-derivative patterns appear for the Raman lines about 1610 cm^{-1} and 1325 cm^{-1}, indicating a spectral shift toward decreased wavenumber when PTAA interacts with PEAI. The red shifts of these skeletal Raman modes provide evidence that PTAA undergoes some structural changes through the π-π interaction with the phenyl ring of PEAI to decrease the vibrational wavenumbers of the Raman-active modes. The tensile strain [25], of the PTAA surface hence became softened by the decreased hydrophobicity induced by PEAI so as to give a red shift of the Raman lines. Fig. 3b shows FTIR spectra of pristine PTAA and the PTAA-PEAI films. The C = C stretching vibrational mode of the aromatic group (phenyl ring) appears in spectral range 1650–1450 cm^{-1}, which is related to the molecular symmetry and the difference of adjacent groups [26]. For PTAA, there are two characteristic IR absorption signals at 1600 and 1500 cm^{-1}. Due to the strong π − π interaction between PTAA and PEAI, the FTIR spectrum of the PTAA-PEAI film shows a clear red shift at the absorbance line about 1500^{-1} with enhanced intensity, a spectral feature similar to what we observed in the Raman spectra.

We measured soft X-ray absorption spectroscopy (XAS) in the beamline TLS 20A1 at NSRRC. Fig. 3c shows XAS of carbon spectra for the films made of only PTAA and PEAI treated PTAA, with the major signal of the carbon sp^2 π* peak located at 285.20 eV [27,28,29]. Compared with PTAA, the sp^2 π* peak of PTAA-PEAI is sharp and intense, indicating that π-π stacking effect contributes more for the latter than for the former.

Other evidence for the π-π stacking effect was found from X-ray photoelectron spectra (XPS) using varied excitation energies, recorded in beamline TLS 24A1 in NSRRC, Taiwan. In this way, bonding information on a nanometer scale was obtained for the PTAA-PEAI film. Fig. 3d shows carbon spectra of PTAA-PEAI with excitation energy of 750 eV, each PEAI molecule contains one phenyl ring, C–C and C-N single bonds that can be resolved from XPS with binding energies 284.9, 285.5 and 286.1 eV corresponding to characteristic XPS signals for sp^2(C = C), sp^3(C–C) and sp^3(C-N), respectively. As shown in Figure S7, we also

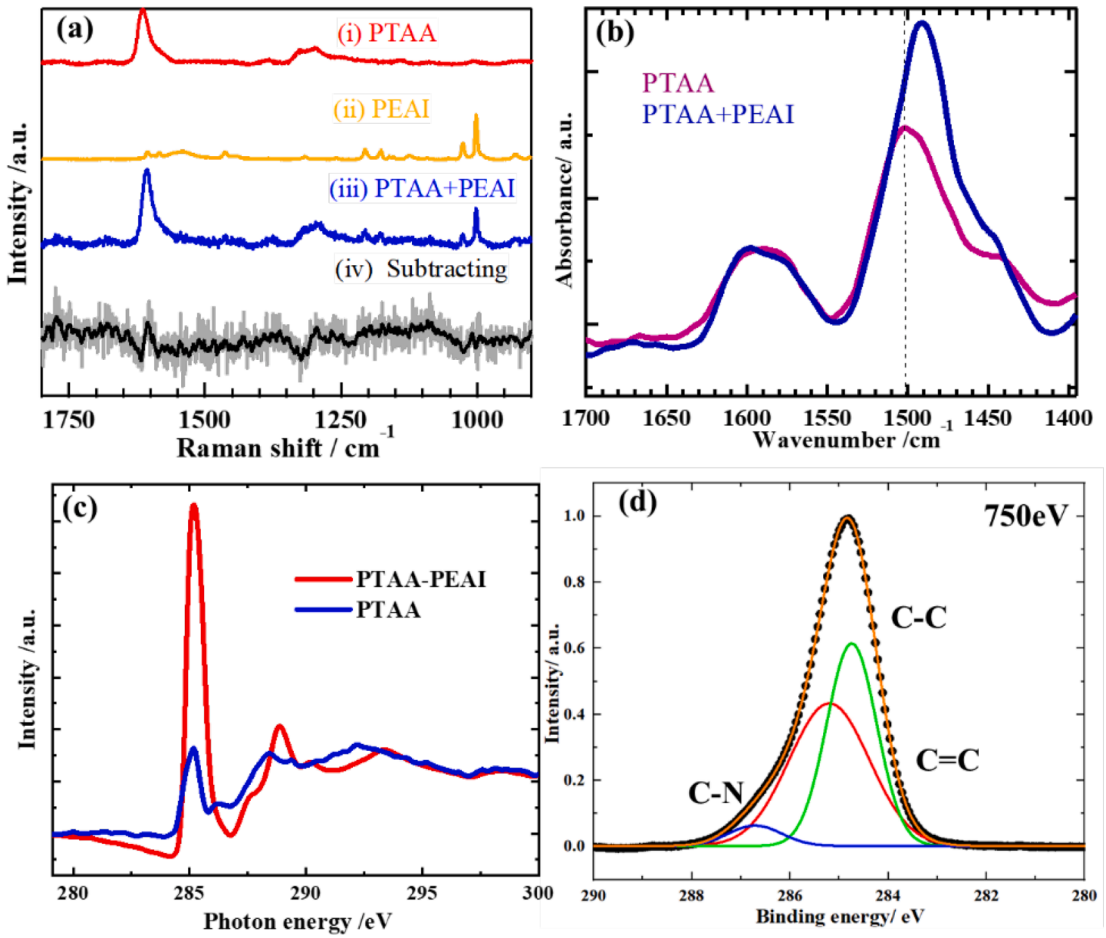

Fig. 3. (a) Raman spectra of (i) pure PTAA, (ii) pure PEAI and (iii) PTAA + PEAI films; grey trace (iv) shows spectrum with (iii) subtracted from (i) and (ii); the black solid trace shows the spectrum after curve smoothing. (b) FTIR spectra of pure PTAA (purple curve) and stacked PTAA + PEAI (blue curve). (c) K-edge XAS spectra of pure PTAA (blue curve) and PEAI treated PTAA (red curve) films. (d) XPS of the PTAA-PEAI film on carbon characteristic bands with excitation energy 750 eV; the XPS bands corresponding to C = C, C–C and C-N bonding are shown as green, red and blue curves, respectively.

recorded the carbon spectra of PTAA-PEAI with excitation energy from 550 eV to 700 eV in step 50 eV. We observed that the intensities of the sp^2(C = C) bands decreased systematically upon increasing the excitation energies toward deeper profile of the film, indicating that the PEAI molecules are aligned in the same direction on the surface to interact with PTAA through a interaction.

Figures S8a and b show XPS of tin element of $FASnI_3$ fabricated with the two-step method with perovskite films deposited on PTAA without and with PEAI pretreatment, respectively. With the help of PEAI pretreatment, the content of Sn^{2+} increased relative to that without PEAI pretreatment, indicating fewer tin(IV) defects being produced for the perovskite crystals made of the PTAA-PEAI film. The UV–vis and PL spectra shown in Figure S9 display no difference between these two samples, but the defects produced in the perovskite film without PEAI modification might cause defect-induced charge recombination so as to decrease the PL lifetime. As the results in Figure S10 show, we measured the PL lifetimes of these two samples using the time-correlated single-photon-counting (TCSPC) technique. The PL temporal profiles exhibit a double-exponential decay feature; the fitted results are summarized in Table S2. The tin perovskite deposited on pristine PTAA shows a lifetime (18 ns) smaller than that of the PTAA-PEAI film (20 ns), confirming that the latter contains fewer defects to inhibit non-radiative recombination than for the former.

The potential-energy levels of each layer in TPSC are important factors to affect the device performance. Accordingly, we measured ultraviolet photoelectron spectra (UPS) of perovskites fabricated on PTAA only and on PTAA-PEAI films; the UPS raw data are presented in Figure S11 for comparison. We found that the relative energies of the valence-band maximum (VBM) and the conduction-band minimum (CBM) for tin perovskite on pristine PTAA layer are −6.2 eV and −4.8 eV, respectively. After PEAI pretreatment, the VBM and CBM of $FASnI_3$ increased to −5.2 eV and −3.8 eV, respectively. The VBM level of tin perovskite with PEAI pretreatment (-5.2 eV) matches well with the HOMO of PTAA (-5.1 eV), feasible for solar-cell applications.

The device configuration and the corresponding potential-energy level diagram are shown in Fig. 4a and b, respectively. In addition to the surface passivation with PEAI, three other organic ammonium iodide salts, butylammonium iodide (BAI) [20], allylammonium iodide (ALAI) [20], and phenylhydrazinium thiocyanate (PHSCN) [4], (Fig. 4c), were applied to modify the surface of PTAA. Figure S12 shows plots of the contact angle of the SnI_2/DMSO precursor solution dropped onto the surfaces of PTAA pretreated with BAI, ALAI and PHSCN, for which the contact angles were 15.67°, 16.65° and 11.87°, respectively. The contact angle was only 5.97° for the PTAA-PEAI film. As a result, we obtained a systematic trend of device performance (Fig. 4d) showing PCE of PEAI (8.3 %) > PHSCN (5.4 %) > ALAI (4.2 %) > BAI (2.7 %) > no treatment (1.5 %), with values of V_{OC} showing the same trend. Note that the performance of the PEAI device has significantly enhanced by a factor of 6.8 in comparison with that without PEAI pretreatment (8.3 vs. 1.5 %). This performance trend is consistent with the trend of the contact angles and reveals a significant role for the π-π interaction between PTAA and organic ammonium salts. For BAI, as no bond is involved, the device

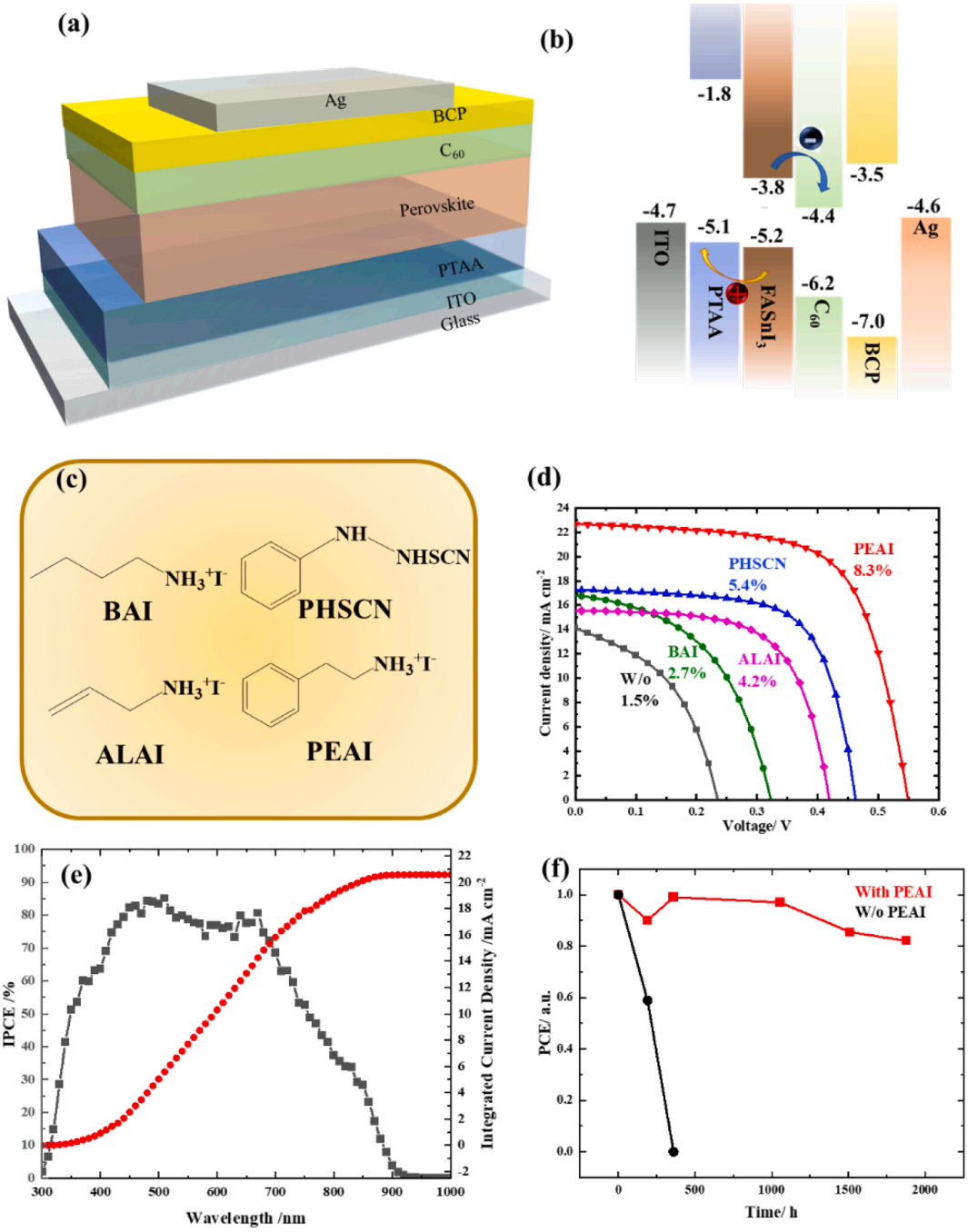

Fig. 4. (a) Inverted TPSC device configuration, (b) potential-energy level diagram for each layer in the device, (c) molecular structures of BAI, ALAI, PHSCN and PEAI, (d) *J-V* characteristic of TPSC fabricated on pristine PTAA, PTAA-BAI, PTAA-ALAI, PTAA-PHSCN and PTAA-PEAI films with corresponding efficiencies as indicated, (e) IPCE spectrum and integrated current density of the PTAA-PEAI device and (f) enduring stability of the TPSC devices made of pristine PTAA and PTAA-PEAI films.

performance is poor; ALAI has one bond but the π-π interaction is too weak to promote much the efficiency. PHSCN was shown to be an efficient surface passivator [4]; it has a phenyl ring to interact with PTAA. As the PH cation has no ammonium cationic terminal, its interaction with the perovskite precursors limited the device performance to be worse than that of the PEAI device. PEAI was found the best reagent to modify the surface of PTAA to make a PTAA-based TPSC with the performance (8.3 %) outperforming that made of PEDOT:PSS as a HTL by either a one-step (7.4 %) [18], or a two-step (6.8 %) [16], approach without considering additional surface passivator for tin perovskite or a 3D/2D device configuration.

Space-charge limited current (SCLC) measurements were exploited to characterize hole mobility of the tin perovskite deposited on PTAA and PTAA-PEAI films. Hole-only devices of ITO/PTAA/$FASnI_3$/Al and ITO/PTAA/PEAI/$FASnI_3$/Al were utilized to measure the hole mobility. As shown in Figure S13, the PTAA and PTAA-PEAI devices exhibit hole mobilities of 4.46×10^{-3} $cm^2V^{-1}s^{-1}$ and 7.36×10^{-3} $cm^2V^{-1}s^{-1}$, respectively. Apparently, the hole mobility of the device made of PEAI-treated PTAA outperforms that made of only PTAA. The integration of the IPCE spectrum of the PEAI device (Fig. 4e) with solar-flux fluence gave current density ~ 21 mA cm^{-2}, agreeing well with that obtained from the *J-V* scan shown in Fig. 4d. Great reproducibility of the PEAI device is shown in the statistical plots of photovoltaic parameters in Figure S14. We found that no effect of hysteresis was found for the best

performing device (Figure S15). The PEAI device stored in a glovebox for 2000 h shows excellent stable performance and retained over 87 % of its initial efficiency, as shown in Fig. 4f. Humidity stability of the PTAA-PEAI device was measured in ambient air condition (RH ~ 50%) to compare with the PEDOT:PSS device, the corresponding results are shown in Figure S16, which indicated that TPSC made of PTAA is more stable than that of PEDOT:PSS in moist environment. Although the surface of PTAA is hydrophobic, using our two-step approach together with surface modification via an effective organic ammonium salt, we for the first time fabricated a workable TPSC device with great device performance. The present work not only provides an example of a hydrophobic hole-selective polymer PTAA to work for TPSC, but also opens a new door to enhance the device performance and stability for TPSC using many other potential *p*-type materials as HTL to match the energy levels between tin perovskite and the HTL.

In conclusion, a tin-perovskite solar cell is a prospective candidate to serve lead-free photovoltaic applications. The best TPSC attained PCE ~ 15 % [7], which is far below its theoretical limit, ~33 % [30]. In addition to the problem of Sn^{2+}/Sn^{4+} oxidation [3,28,30,31], the matching of energy levels between perovskite and charge-transport layers is an issue to be addressed. The traditional high-performance inverted TPSC were fabricated based on a hydrophilic PEDOT:PSS HTL using a one-step antisolvent approach, for which the hygroscopic PEDOT:PSS with poor environmental stability limits its further development. Herein we report the first successful example to grow a tin-perovskite layer on a hydrophobic PTAA surface. We found that modification of the PTAA surface with a suitable bulky organic ammonium salt is an important step to make a hydrophilic surface for feasible deposition of a tin-perovskite layer via a two-step approach. Through an effective π-π interaction with PTAA, the surface modification with the PEAI salt enabled the TPSC to attain PCE 8.3 % with great stability upon storage in darkness. In addition to PTAA, many other HTL materials can be tested with tin perovskites of varied types for the purpose of energy-level alignment between perovskite and HTL to enhance their device performance and stability. Work is in progress along this direction.

Declaration of Competing Interest

The authors declare the following financial interests/personal relationships which may be considered as potential competing interests: Eric Wei-Guang Diau reports a relationship with Ministry of Science and Technology, Taiwan that includes: funding grants.

Data availability

No data was used for the research described in the article.

Acknowledgements

We thank Prof. U-Ser Jeng (NSRRC) and his group members for their kind assistance in GIWAXS data analysis. We also thank Prof. C.S. Lin and Ms. Y.T. Lee of Instrumentation Center, National Taiwan University for FEG-SEM experiments. This work is supported by Ministry of Science and Technology (MOST 110-2123-M-A49-001 and MOST 111-2634-F-A49-007) and Center for Emergent Functional Matter Science of National Yang Ming Chiao Tung University (NYCU) from The Featured Areas Research Center Program within the framework of the Higher Education Sprout Project by Ministry of Education (MOE) in Taiwan. National Synchrotron Radiation Research Center, Hsinchu Science Park, Taiwan, provided beam time for measurements of XAS, energy-dependent XPS and GIWAXS spectra.

Appendix A. Supplementary data

Supplementary data to this article can be found online at https://doi.org/10.1016/j.cej.2022.138037.

References

[1] H. Min, D.Y. Lee, J. Kim, G. Kim, K.S. Lee, J. Kim, M.J. Paik, Y.K. Kim, K.S. Kim, M. G. Kim, T.J. Shin, S. Il Seok, Perovskite solar cells with atomically coherent interlayers on SnO_2 electrodes, Nature 598 (7881) (2021) 444–450.
[2] Y. Vaynzof, Long live the perovskite module, Nat. Energy 6 (6) (2021) 578–579.
[3] E.-G. Diau, E. Jokar, M. Rameez, Strategies to improve performance and stability for tin-based perovskite solar cells, ACS Energy Lett. 4 (8) (2019) 1930–1937.
[4] E. Jokar, H.-S. Chuang, C.-H. Kuan, H.-P. Wu, C.-H. Hou, J.-J. Shyue, E. Wei-Guang Diau, Slow passivation and inverted hysteresis for hybrid tin perovskite solar cells attaining 13.5% via sequential deposition, J. Phys. Chem. Lett. 12 (2021) 10106–10111.
[5] X. Jiang, H. Li, Q. Zhou, Q.i. Wei, M. Wei, L. Jiang, Z. Wang, Z. Peng, F. Wang, Z. Zang, K. Xu, Y.i. Hou, S. Teale, W. Zhou, R. Si, X. Gao, E.H. Sargent, Z. Ning, One-step synthesis of SnI2·(DMSO)x adducts for high-performance tin perovskite solar cells, J. Am. Chem. Soc. 143 (29) (2021) 10970–10976.
[6] E. Jokar, C.H. Chien, C.M. Tsai, A. Fathi, E.W.G. Diau, Robust tin-based perovskite solar cells with hybrid organic cations to attain efficiency approaching 10%, Adv. Mater. 31 (2019) 1804835.
[7] B.B. Yu, Z. Chen, Y. Zhu, Y. Wang, B. Han, G. Chen, X. Zhang, Z. Du, Z. He, Heterogeneous 2D/3D tin-halides perovskite solar cells with certified conversion efficiency breaking 14%, Adv. Mater. 33 (2021) 2102055.
[8] E. Jokar, P.H. Hou, S.S. Bhosale, H.S. Chuang, S. Narra, E. Wei-Guang Diau, Mixing of azetidinium in formamidinium tin triiodide perovskite solar cells for enhanced photovoltaic performance and high stability in air, ChemSusChem 14 (2021) 4415–4421.
[9] X. Liu, T. Wu, X. Luo, H. Wang, M. Furue, T. Bessho, Y. Zhang, J. Nakazaki, H. Segawa, L. Han, Lead-free perovskite solar cells with over 10% efficiency and size 1 cm2 enabled by solvent-crystallization regulation in a two-step deposition method, ACS Energy Lett. 7 (1) (2022) 425–431.
[10] A.A. Said, J. Xie, Q. Zhang, Recent progress in organic electron transport materials in inverted perovskite solar cells, Small 15 (2019) 1900854.
[11] M. Wang, W. Li, H. Wang, K. Yang, X. Hu, K. Sun, S. Lu, Z. Zang, Small molecule modulator at the interface for efficient perovskite solar cells with high short-circuit current density and hysteresis free, Adv. Electron. Mater. 6 (2020) 2000604.
[12] W. Li, H. Wang, X. Hu, W. Cai, C. Zhang, M. Wang, Z. Zang, Sodium benzenesulfonate modified poly (3,4-ethylenedioxythiophene): polystyrene sulfonate with improved wettability and work function for efficient and stable perovskite solar cells, Sol. RRL 5 (2021) 2000573.
[13] X. Sun, X. Deng, Z. Li, B. Xiong, C. Zhong, Z. Zhu, Z.A. Li, A.K.Y. Jen, Dopant-free cross conjugated hole-transporting polymers for highly efficient perovskite solar cells, Adv. Sci. 7 (2020) 1903331.
[14] S. Wu, J. Zhang, Z. Li, D. Liu, M. Qin, S.H. Cheung, X. Lu, D. Lei, S.K. So, Z. Zhu, A.-Y. Jen, Modulation of defects and interfaces through alkylammonium interlayer for efficient inverted perovskite solar cells, Joule 4 (6) (2020) 1248–1262.
[15] X. Zheng, Y.i. Hou, C. Bao, J. Yin, F. Yuan, Z. Huang, K. Song, J. Liu, J. Troughton, N. Gasparini, C. Zhou, Y. Lin, D.-J. Xue, B. Chen, A.K. Johnston, N. Wei, M. N. Hedhili, M. Wei, A.Y. Alsalloum, P. Maity, B. Turedi, C. Yang, D. Baran, T. D. Anthopoulos, Y.u. Han, Z.-H. Lu, O.F. Mohammed, F. Gao, E.H. Sargent, O. M. Bakr, Managing grains and interfaces via ligand anchoring enables 22.3%-efficiency inverted perovskite solar cells, Nat. Energy 5 (2) (2020) 131–140.
[16] S. Shahbazi, M.-Y. Li, A. Fathi, E.-G. Diau, Realizing a cosolvent system for stable tin-based perovskite solar cells using a two-step deposition approach, ACS Energy Lett. 5 (8) (2020) 2508–2511.
[17] D. Song, S. Narra, M.-Y. Li, J.-S. Lin, E.-G. Diau, Interfacial engineering with a hole-selective self-assembled monolayer for tin perovskite solar cells via a two-step fabrication, ACS Energy Lett. 6 (12) (2021) 4179–4186.
[18] E. Jokar, C.-H. Chien, A. Fathi, M. Rameez, Y.-H. Chang, E.-G. Diau, Slow surface passivation and crystal relaxation with additives to improve device performance and durability for tin-based perovskite solar cells, Energy Environ. Sci. 11 (9) (2018) 2353–2362.
[19] M. Wang, H. Wang, W. Li, X. Hu, K. Sun, Z. Zang, Defect passivation using ultrathin PTAA layers for efficient and stable perovskite solar cells with a high fill factor and eliminated hysteresis, J. Mater. Chem. A 7 (46) (2019) 26421–26428.
[20] E. Jokar, P.-Y. Cheng, C.-Y. Lin, S. Narra, S. Shahbazi, E. Wei-Guang Diau, Enhanced performance and stability of 3D/2D tin perovskite solar cells fabricated with a sequential solution deposition, ACS Energy Lett. 6 (2021) 485–492.
[21] S. Pratap, F. Babbe, N.S. Barchi, Z. Yuan, T. Luong, Z. Haber, T.-B. Song, J.L. Slack, C.V. Stan, N. Tamura, C.M. Sutter-Fella, P. Müller-Buschbaum, Out-of-equilibrium processes in crystallization of organic-inorganic perovskites during spin coating, Nat. Commun. 12 (1) (2021).
[22] J. Ogle, D. Powell, E. Amerling, D.-M. Smilgies, L. Whittaker-Brooks, Quantifying multiple crystallite orientations and crystal heterogeneities in complex thin film materials, CrystEngComm 21 (38) (2019) 5707–5720.
[23] C. Kvarnström, A. Petr, P. Damlin, T. Lindfors, A. Ivaska, L. Dunsch, Raman and FTIR spectroscopic characterization of electrochemically synthesized poly (triphenylamine), PTPA, J. Solid State Electrochem. 6 (2002) 505–512.
[24] R.E. Littleford, D.R. Tackley, J.C. Cherryman, G. Dent, W.E. Smith, A Raman and DFT study of substituted triphenylamines for use as charge transfer materials in light emitting polymers, J. Mol. Struct 692 (1-3) (2004) 81–90.
[25] J. Xu, J. Dai, H. Dong, P. Li, J. Chen, X. Zhu, Z. Wang, B. Jiao, X. Hou, J. Li, Surface-tension release in PTAA-based inverted perovskite solar cells, Org. Electron 100 (2022), 106378.
[26] N. Colthup, Introduction to infrared and Raman spectroscopy, Elsevier (1990) 261–288.

[27] A. Batra, G. Kladnik, H. Vázquez, J.S. Meisner, L. Floreano, C. Nuckolls, D. Cvetko, A. Morgante, L. Venkataraman, Quantifying through-space charge transfer dynamics in π-coupled molecular systems, Nat. Commun. 3 (2012) 1–7.
[28] M. Linares, S. Stafström, P. Norman, Effects of π-stacking interactions on the near carbon K-edge x-ray absorption fine structure: A theoretical study of the ethylene pentamer and the phthalocyanine dimer, J. Chem. Phys. 130 (2009), 104305.
[29] J. Zhong, H. Zhang, X. Sun, S.-T. Lee, Synchrotron soft X-ray absorption spectroscopy study of carbon and silicon nanostructures for energy applications, Adv. Mat. 26 (46) (2014) 7786–7806.
[30] X. Jiang, Z. Zang, Y. Zhou, H. Li, Q. Wei, Z. Ning, Tin halide perovskite solar cells: an emerging thin-film photovoltaic technology, Acc. Mater. Res. 2 (2021) 210–219.
[31] X. Meng, Y. Li, Y. Qu, H. Chen, N. Jiang, M. Li, D.-J. Xue, J.-S. Hu, H. Huang, S. Yang, Crystallization kinetics modulation of FASnI3 films with pre-nucleation clusters for efficient lead-free perovskite solar cells, Angew Chem. 133 (7) (2021) 3737–3742.